A Power Independent Detection Method for Ultra Wide Band (UWB) Impulse Radio Networks

Alaeddine El Fawal, Jean Yves Le Boudec

School of Computer and Communication Sciences, EPFL, Switzerland CH-1015 Lausanne, Switzerland

March 16, 2005

Abstract: We propose a novel detection method for non-coherent synchronization (signal acquisition) in multi-access UWB impulse radio (IR) networks. It is designed to solve the IUI (Inter-User Interference) that occurs in some ad-hoc networks where concurrent transmissions are allowed with heterogeneous power levels. In such scenarios, the conventional detection method, which is based on correlating the received IR signal with a Template Pulse Train (TPT), does not always perform well. Our proposal has similar complexity as the conventional method. We evaluate its performance with the Line Of Sight (LOS) office indoor channel model proposed by the IEEE P802.15.4a study group and find that the improvement is significant.

1 Introduction

We propose a novel detection method, called PID (Power Independent Detection) method, for non-coherent synchronization in multi-access Ultra Wide Band (UWB) Impulse Radio (IR) networks. To understand what we mean by detection method, let us define the following terminology. We consider the synchronization of one receiver to one sender (also called signal acquisition). We are interested in methods based on the correlation of the IR signal with a Template Tulse Train (TPT). Such methods involve two ingredients: (1) the detection, which correlates the received signal with a (TPT) and (2) the search algorithm, which shifts the TPT. We focus on detection. Our proposal aims at solving the extreme Inter-User Interference (IUI) case (near-far problem), when there are multiple interfering transmitters, asynchronous transmissions and heterogeneous power levels. This occurs for example in the presence of multiple interfering piconets, or in purely ad-hoc networks that allow concurrent transmissions, always at full power [4, 13]. In such scenarios the conventional detection method faces a certain failure. Our PID method solves the problem without any additional complexity overhead, e.g. for a digital receiver, it employs the same sampling frequency and number of operations as the conventional detection method. Unlike the conventional detection method, the PID method splits the correlation into elementary correlations, each one corresponds to one pulse in the TPT. Then, two threshold checks are performed. The first is to detect pulses whereas the second is to detect the signal based on the number of detected pulses. To evaluate the performance of the PID method, we propose a hybrid method combining analysis and simulation that is carried out according to the Line Of Sight (LOS) office indoor channel model proposed by the IEEE P802.15.4a study group [2]. The results presented in the end show a significant improvement compared to the con-

ventional detection method.

The conventional detection method (detailed in 3.1) has been recently adopted in a large number of references, in combination with a variety of search algorithms; Some search algorithms are adequate for fine grained synchronization (e.g. serial [16]) or for coarse synchronization (e.g. "Look and Jump", Bit reversal [1, 10, 11], sequential block search [7] and n-scaled acquisition algorithms [17]). It suffers from the near-far problem with all these search algorithms. The PID method, is designed to replace it and solve the near-far problem with all the search algorithms. Further, the PID method can be generalized to all correlation-based synchronization methods (e.g. conventional one and others such as Differential Detector [9, 15, 20]) and it can be even used with a rake detector as proposed in [19], which do not operate well in case of near-far problem.

2 Model and Assumption:

An IR signal consists of trains of very short pulses to the order of a nanosecond or even a sub-nanosecond. In this paper we consider a TH (Time Hopping) physical layer proposed by Win-Scholtz [21]. TH is ensured using a pseudo-random code of length L_c. Such a physical layer can employ several modulation schemes such as BPSK (Binary Phase Shift Keying), PPM (Pulse Position Modulation), PAM (Pulse Amplitude Modulation); we do not have to specify a modulation scheme here since there is no data transmitted during the synchronization period and thus the signal we treat is not modulated. The transmitted signal of the mth user is:

$$s^{(m)} = A^{(m)} \sum_j \sum_{k=1}^{L_c}$$
$$p\left(t - (c_k^{(m)} - 1)T_c - (k-1)T_f - jT_s - \tau_X^{(m)}\right) \quad (1)$$

where $p(t)$ is the second derivative of the Gaussian pulse (Appendix A), $A^{(m)}$ is to indicate the signal amplitude, T_c is the chip duration, $c_k^{(m)}$ is the kth element of the mth user code, i.e. the number of the chip that corresponds to the pulse position in the kth frame of a mth user sequence, $T_f = N_c \times T_c$ is the frame duration where N_c is the number of chips in one frame, T_s is the sequence duration, that is $T_s = T_f \times L_c$ and $\tau_X^{(m)}$ is the transmission start time. We assume that the pulse width and the chip duration are equal.

For our results, we consider the SV (Saleh-Valenzuela) channel model adopted in [2]. For simplicity, we express its impulse response using the well-known tapped delay line expression:

$$h(t) = \sum_{l=1}^{L} a_l \delta(t - t_l) \quad (2)$$

1

where $\delta(t)$ denotes the Dirac impulse, t_l the signal delay along the lth path and a_l is a real propagation coefficient that includes the channel attenuation and the polarity of the signal along the lth path. Then the received signal is given by:

$$r(t) = \sum_{m=1}^{M} \sum_{l=1}^{L} a_l^{(m)} s^{(m)} \left(t - t_l^{(m)} \right) + n(t) \qquad (3)$$

where M is the number of users in the network and $n(t)$ is the White Gaussian noise.

Assume that the receiver is interested in detecting the signal sent by the first user. Then, the objective of the synchronization methods that use either the PID or the conventional detection methods is to detect whether the first user is transmitting or not, and if he is transmitting, they find the arrival time of one sequence in the first user signal according to one of the multipath components, i.e. they find one value of $\left\{ \left(\tau_X^{(1)} + jT_s + t_l^{(1)} \right), l = 1, \ldots, L, j = 0, 1, \ldots \right\}$, let τ_0 be the found value. Further it detects the sign of the corresponding a_l.

3 Conventional Detection Method

3.1 Description

As it is explained in 1, we consider synchronization methods that involve two ingredients: the detection and the search algorithm. With the conventional detection method, the received IR signal is correlated with a TPT, which is a replica of the sequence used by he first user and which is given by:

$$s_{TPT}(t) = \sum_{k=1}^{L_c} p \left(t - (c_k^{(1)} - 1)T_c - (k-1)T_f \right) \qquad (4)$$

The idea behind the correlation is to compare the TPT with the received impulse radio signal, which may or may not have the identical pattern of pulses as the TPT. Then a threshold check is performed on the output of the correlation (β in Eq. 5) to detect whether there is a match (an alignment) between the TPT and the received IR signal.

The role of the search algorithm is to shift the TPT with predefined time offsets so that the TPT is placed at various locations in time as compared to the received impulse radio signal until a match is obtained between them, i.e. they are aligned. The output of the cross-correlator is:

$$\beta = \int_{\sum_{i=1}^{n} \text{Offset}_i}^{\sum_{i=1}^{n} \text{Offset}_i + T_s} r(t) \times s_{TPT} \left(t - \sum_{i=1}^{n} \text{Offset}_i \right) dt \qquad (5)$$

where n is the current shift number and Offset_i is the time offset at the ith shift of the TPT. Eq. 5 is known in the literature as a coherent integration, but in this paper we refer to it as a correlation between the TPT and the received IR signal (note that we do not assume that the receiver knows the channel). The receiver gets synchronized with the transmitter at the nth offset if $\sum_{i=1}^{n} \text{Offset}_i$ is equal to one value of the set $\left\{ \left(\tau_X^{(1)} + jT_s + t_l^{(1)} \right), l = 1, \ldots, L, j = 0, 1, \ldots \right\}$, and thus $\tau_0 = \sum_{i=1}^{n} \text{Offset}_i$. Notice that, according to Eq. 4, Eq. 5 can be interpreted as L_c elementary correlations $\{(\alpha_k)\}$, $k = 1, \ldots, L_c$. α_k is the output of the elementary correlation k that corresponds to the kth pulse in the TPT. We can write:
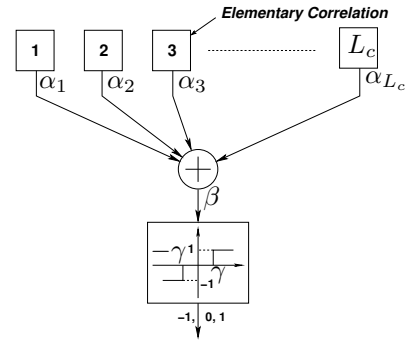
$$\beta = \sum_{k=1}^{L_c} \alpha_k , \qquad (6)$$

Figure 1: The conventional detection method can be interpreted as L_c elementary cross-correlations. Block i, $i = 1, \ldots, L_c$, presents the correlation of the ith pulse in the TPT with its corresponding interval.

where:

$$\alpha_k = \int_{(c_k^{(1)}-1)T_c+(k-1)T_f+\sum_{i=1}^{n} \text{Offset}_i}^{(c_k^{(1)}-1)T_c+(k-1)T_f+\sum_{i=1}^{n} \text{Offset}_i+T_c} p \left(t - (c_k^{(1)} - 1)T_c \right.$$
$$\left. -(k-1)T_f - \sum_{i=1}^{n} \text{Offset}_i \right) \times r(t) dt \qquad (7)$$

These L_c elementary correlations correspond to the L_c correlations of the TPT *pulses* and their corresponding intervals of the IR signal. In Fig. 1, the L_c elementary correlations are presented by the blocks indexed from 1 to L_c. β is the input of the decision block, which in turn performs a threshold check. Hence, a match between the TPT and the IR signal is declared if the absolute value of β exceeds certain threshold γ. Note that a (-1) output of the decision block means that a match is declared but the signal is inverted due to reflection, i.e. the corresponding a_l is negative (see previous section).

3.2 Example Showing the Problem with the Conventional Detection Method

To show the inefficiency of the conventional detection method, we present one scenario that is based on the measurement made by M. Win and R. Scholtz in [22] for an indoor environment. Consider a source (user 1) that is 10 m from the receiver. The measurement in [22] gives that the amplitude of the strongest source pulse seen by the receiver is in the order of 0.03V. Assume now that there is an interferer (user 2) that is 1m from the receiver. The measured amplitude of the interfering pulse is of 1V, 33 times higher than the source pulse. Refer by $A_r^{(1)}$ ($A_r^{(2)}$ respectively) to the source (interferer respectively) signal amplitude at the receiver, we have $A_r^{(2)} \approx 33 A_r^{(1)}$. Let $\alpha_0^{(1)}$ ($\alpha_0^{(2)}$ respectively) be the output of the correlation between one source (interferer respectively) pulse and one TPT pulse when they are aligned, we can write:

$$\alpha_0^{(1)} = A_r^{(1)} \int_0^{T_c} p^2(t) dt = \frac{A_r^{(2)}}{33} \int_0^{T_c} p^2(t) dt \approx \frac{\alpha_0^{(2)}}{33} \qquad (8)$$

$\alpha_0^{(2)}$ is 33 times larger than $\alpha_0^{(1)}$. Note that when the source signal and the TPT are perfectly aligned, neglecting the interference and noise effects, β is equal to $L_c \times \alpha_0^{(1)}$. Consequently, γ can not be larger than $L_c \times \alpha_0^{(1)}$, otherwise the source signal can not be detected. If $L_c \leq 33$, it is sufficient to have one interfering pulse aligned with one TPT pulse to get a false alarm. More explanations are given in Appendix B.

2

To avoid this false alarm, but still using the conventional detection method, L_c must be much larger than 33, which would be an extremely unaffordable overhead in term of synchronization time, since the synchronization time is proportional to the code length L_c [5]. Note that, when the number of concurrent transmissions increases, the situation becomes worse.

To summarize this example, the synchronization is either unfeasible or entails an extremely large overhead using the conventional detection method in none-power control IR networks when concurrent transmissions are allowed.

4 Our Proposal: Power-Independent Detection Method

The idea behind the cross-correlation between the TPT and the IR signal is to detect a match between them. We need to find in the IR signal L_c pulses that have the same pattern as the TPT. But the conventional detection method does not do this. It looks at the energy captured by the correlation between the TPT and the received IR signal, which is indicated by β in Fig. 1, regardless of its distribution over the L_c elementary correlations. So, if this energy, β, is larger than the threshold, we say that the synchronization is achieved. But what about if all the energy comes from one elementary correlation, e.g. $\beta = \alpha_1$ and $\alpha_k = 0$, $k = 2, \ldots, L_c$? This is the bug in the scenario shown in section 3.2 in the case where $L_c \leq 33$. Unlike the conventional de-
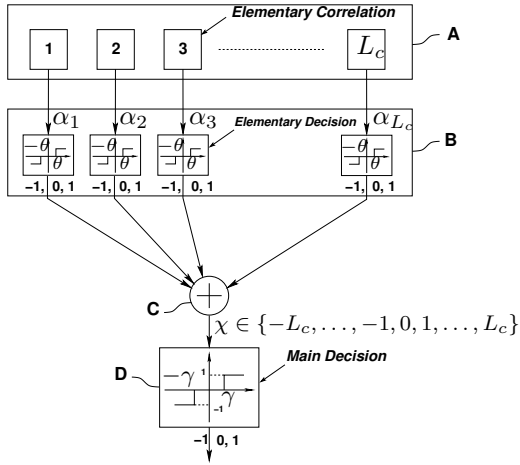

Figure 2: PID method: each pulse is detected based on an elementary decision block. The final detection decision is based on the number of pulses detected.

tection method, the PID method solves the problem by looking at the individual energy captured by each elementary correlation separately, i.e. by looking at each α_k separately, $k = 1, \ldots, L_c$. Fig. 2 describes the architecture of our proposal; the output of each elementary correlation α_k, $k = 1, \ldots, L_c$, passes through an elementary decision block that performs a threshold check. If the absolute value of α_k is larger than θ, then a pulse is detected and the output of the elementary decision block k will be 1 or -1 depending on the sign of α_k (-1 means the detected pulse has negative polarity). Otherwise it will be 0. Let χ be the sum of the L_c *Elementary Decision* block outputs, we have:

$$\chi = \sum_{k=1}^{L_c} \left(\mathbf{1}_{\{\alpha_k \geq \theta\}} - \mathbf{1}_{\{\alpha_k \leq -\theta\}} \right) \in \{-L_c, \ldots, 0, \ldots, L_c\} \quad (9)$$

If the absolute value of χ is larger than the main threshold mTh, the output of the main decision block will be 1 or -1 (detected path is with negative polarity) and thus a match will be declared between the IR signal and the TPT. In the opposite case the output of the main decision block will be 0. mTh should be a natural number less than L_c.

It is intuitively clear that this new method should solve the problem described in section 3.2; it is designed for an environment without power control since it is sensitive to the existence of a pulse not to its power (assuming it has enough energy to be detected). So we call our proposal "Power-Independent Detection".

5 Performance Evaluation Method

We evaluate the performance of PID and compare it to the conventional detection method.

5.1 How to Evaluate the Performance

For a meaningful performance evaluation of the conventional detection and the PID methods, we imbedded them in a complete synchronization method, which consists an identification phase, followed by a verification phase. Each phase uses the two aforementioned ingredients of detection and search algorithm iteratively. For the latter, we adopted serial search. This is because we aim to evaluate the performance of the PID method independently of the impact of optimizations that use coarse synchronization.

The Complete Synchronization Method: When the complete synchronization method uses PID, we call it "PID synchronization method"; when it uses conventional detection, we call it "conventional synchronization method".

Let N be the number of the search bins (Appendix F); let "true sequence" be the sequence to be detected in the received IR signal; it has the same pattern as the TPT at the receiver.

The PID synchronization method consists of two phases (the flowchart is shown in Appendix C). In the first phase, the procedure in Fig. 2 without the main decision block, i.e. block D, is repeated for the N search bins according to the serial search algorithm; we start with bin 1, then bin 2 till bin N. The largest χ, χ_{max}, is memorized, as well as its corresponding search bin. Then χ_{max} is compared to a first mean threshold, mTh1. If the absolute value of χ_{max} is strictly above mTh1, the bin that corresponds to χ_{max} is considered as a signal bin, SB, and we move to the second phase. Otherwise, the procedure of the first phase starts anew.

In the second phase we aim to verify the detection of the first phase. It consists of A iterations, in each one the procedure is the same as in the first phase but on a predefined neighborhood of SB, V, including SB, instead of the whole N bins, and with a second mean threshold, mTh2, that is larger than mTh1. If at least B threshold checks among A succeed, the detection is confirmed, otherwise the detection of the first phase is cancelled and the procedure of the first phase starts anew.

The conventional synchronization method is similar to the PID synchronization method with the difference that it does not per-

form a threshold check on the elementary correlation outputs.

Performance Metrics: We measure the performance of each procedure by the following metrics, applied to the synchronization method: (1) the complement of the probability of Good Detection ($\overline{P_{GD}} = 1 - P_{GD}$) in the presence of the true sequence in the received IR signal (2) the probability of false alarm, P_{FA0}, in the absence of the true sequence in the received IR signal and (3) the total error defined as $E_t = \overline{P_{GD}} + P_{FA0}$. Note that the probability of false alarm in the presence of the true sequence is included in $\overline{P_{GD}}$ and it does not give additional information about the total error, hence, for brevity, we do not consider it here as a metric.

5.2 Computation of Metric Using Hybrid Method: Analysis + Simulation

5.2.1 Analysis:

The goal of the analysis is to express the metrics as functions of other probabilities that we obtain by simulation. The probabilities are as follows: During the first phase we have P_1, the probability of good detection when the received IR signal contains the true sequence, and P_2, the probability of a bad detection when the received IR signal does not contain the true sequence. During the second phase we define P_3 as the probability that one threshold check succeeds, given that the first phase has resulted in a good detection in the presence of the true sequence and P_4 as the Probability that one threshold check succeeds, given that the first phase has resulted in a bad detection in the absence the true sequence.

The Analysis presented in Appendix D gives:

$$\overline{P_{GD}} = 1 - P_1 \sum_{i=B}^{A} \binom{A}{i} P_3^i (1-P_3)^{(A-i)} \qquad (10)$$

$$P_{FA0} = P_2 \sum_{i=B}^{A} \binom{A}{i} P_4^i (1-P_4)^{(A-i)} \qquad (11)$$

5.2.2 Simulation:

In order to compute the metrics, we ran a campaign of simulations to estimate the probabilities P_i, $i = 1, \ldots, 4$. The simulations were carried out using matlab. We tried to make the simulated scenario as realistic as possible by choosing a real multipath fading channel model and by adjusting all simulation parameters, e.g. the bit energy to noise spectral density ratio E_0/N_0 (one bit corresponds to one pulse), the physical layer parameters, the transmission power levels, the number of users.

Channel Model: The simulations were carried out according to the Line Of Site (LOS) indoor office channel model described in [2] for a communication range from 3m to 28m. This model is the fruit of a campaign of industrial and academic contributions. The NLOS (Non LOS) is not considered since its parameter values are not available yet in [2].

Although the measurements made for this model were using an UWB IR signal, the model is generalized to be used by any carrier modulation system. Thus, the phase of a multipath component is considered as uniformly distributed over [0,2π] which is meaningless in an UWB IR baseband transmission. We solve this problem by relaxing this hypothesis and replacing it by the one adopted in [3], which is appropriate for IR baseband transmission. Then, the phase of a multipath component will be $0/\pi$ with an equal probability for representing pulse inversion due to the reflection from different surfaces.

For simplicity, we assume that the distribution of the small scale fading is Rayleigh instead of Nakagami since the mean value in dB of the "m" parameter of the Nakagami distribution in the adopted model is very close to zero, which corresponds to the particular case of the Rayleigh distribution.

Simulation Parameters: We consider that all users are sending non-modulated IR signals, an assumption that does not affect our results since the interferer signals are already random with respect to the receiver and using data modulation will add one more random variable with zero mean. We have $T_c = 0.2ns$. N_c is set to 200 chips that corresponds to $40ns$, which is sufficient to minimize the inter-symbol interference due the multipath delay spread in the LOS indoor office environment [6, 12], in particular we consider a guard time of 100 chips. The sampling frequency is 50 GHz, much larger than the Nycquist sampling frequency, to simulate an analog receiver since the impact of the sampling frequency is out of the scope of this study. The elementary threshold (θ in Fig. 2) is set to $0.5 \times \alpha_0^{(1)}$ (see Eq. 8) with $A_r^{(1)}$ corresponds to the highest multipath components.

Each simulated scenario contains several transmitters, we refer to them as users, the one that is transmitting the true sequence is called the source and others are the interferers. The source signal power observed by the receiver is set to $-30dBm$, whereas the interferer signal powers observed by the receiver are uniformly distributed over [-30dBm, -10dBm]. Then the largest value of signal power that an interferer can have is 20 dB larger than the source signal power. Indeed, according to the pathloss model used in [2], this difference in power corresponds to a communication rage of 17 m approximately (see Appendix E) where all users are transmitting at the same power and the source is the farthest. Such a communication range is typical for an indoor environment and the adopted channel model of [2] is still valid since it is based on measurements that cover a range from 3 m to 28 m.

In all simulated scenarios, E_0/N_0 is computed with respect to the source signal power.

6 Performance Evaluation Results

6.1 Performance Evaluation Results of the PID Synchronization Method

The probabilities P_i, $i = 1, \ldots, 4$, are obtained by simulation. P_1 and P_2 are computed by averaging the results of 200 independent runs for each simulated scenario. A different independent noise realization is computed per run and, within the same run, a different channel realization is computed per user.

To compute P_3 and P_4, the stationarity of the channel during the synchronization should be taken into account. Thus, the computation of P_3 and P_4 is different and more complicated. We proceed as follows: for each run of the 200 runs above, if a detection is declared, 9 other runs are done with the same channel realization for each user but with different noise realization. Then, for a given scenario, if all the 200 runs above result in a detection declaration, we will have 9 additional runs for each run and thus 1800 runs for this scenario.

We ran simulations for E_0/N_0 values between 0 dB and 20 dB, L_c values between 8 and 30, and number of users between 5 and 20 users. In the extreme scenarios with low E_0/N_0 ($< 10dB$), short L_c (< 16) and large number of users (20 users) the performance was not so good due to a huge amount of interference and noise. But, starting from $E_0/N_0 = 10dB$ and $L_c = 16$, the performance is acceptable and the results seem to be similar. For lack of space, we show only one scenario in order to explain the behavior of the PID synchronization method and to show the optimal working point.

Fig. 3 (a), (b) and (c) shows the metrics $\overline{P_{GD}}$, P_{FA0} and E_t (see the legend for details). We tried to draw results for a range of $9 - 19$ for mTh1 and mTh2, but sometimes the values were too small (less than 10e-25) and matlab was not able to draw them. For Fig. 3 (a), the interpretation is as follows: first notice that $\overline{P_{GD}}$ is decreasing with P_3. For a given mTh1, P_3 is a decreasing function of mTh2, whereas P_1 is independent of mTh2. Consequently, $\overline{P_{GD}}$ is an increasing function of mTh2. In contrast, for a given mTh2, P_1 is a decreasing function of mTh1 but P_3 increases with mTh1 since it is a conditional probability that χ_{max} in one iteration of the second phase is above mTh2 given that χ_{max} in the first phase is above mTh1 and the difference between mTh1 and mTh2 decreases when mTh1 increases. Therefore, given mTh2, it is not evident how $\overline{P_{GD}}$ varies according to mTh1 since P_1 and P_3 vary in opposite directions and moreover the values of A and B influence the impact of the variation of P_3. For mTh2 = 18, $\overline{P_{GD}}$ increases with mTh1 when mTh1 goes from 12 to 17, but it decreases when mTh1 passes from 17 to 18. Fig. 3 (b) shows the probability P_{FA0}. To understand the trends of the curves, a similar interpretation can be made as above. For instance, for a given mTh1, P_2 is independent of mTh2 and P_4 is a decreasing function of mTh2. Thus, P_{FA0} decreases with mTh2 for a fixed mTh1. In contrast, for a fixed mTh2, P_2 is decreasing with mTh1 whereas P_4 is increasing.

Fig. 3 (c) shows E_t. The optimal working point for this scenario is for (mTh1;mTh2) = (10;12) where E_t is minimized. On the left hand of the optimal working point, P_{FA0} is dominant and the curves imitate those of P_{FA0} in Fig. 3 (b). In contrast, $\overline{P_{GD}}$ becomes dominant on the right hand of the optimal working point and the curves at this side are similar to those of $\overline{P_{GD}}$ in Fig. 3 (a).

In conclusion, using the PID synchronization method, an optimal working point can be obtained by minimizing E_t. For this specific example, the optimal working point is $mTh1 = 10$, $mTh2 = 12$.

6.2 Comparison between the PID and the Conventional Synchronization Methods:

To show the performance of the conventional complete method, we computed a lower bound of its $\overline{P_{GD}}$. According to Eq. 10, a lower bound of $\overline{P_{GD}}$ is $1 - P_1$, which is independent of the second phase. Further, a lower bound of $1 - P_1$ can be simply obtained by relaxing the mTh1 threshold check in the first phase (which returns as if we set mTh1 to zero). Then, a good detection is obtained if β_{max} (χ_{max} with the PID synchronization method) corresponds to a signal bin without any constraint on its value.

For the conventional complete method, the lower bound of P_1 for a given scenario is obtained by averaging the results of 30 independent runs for this scenario. Fig. 4 (a) shows two curves as
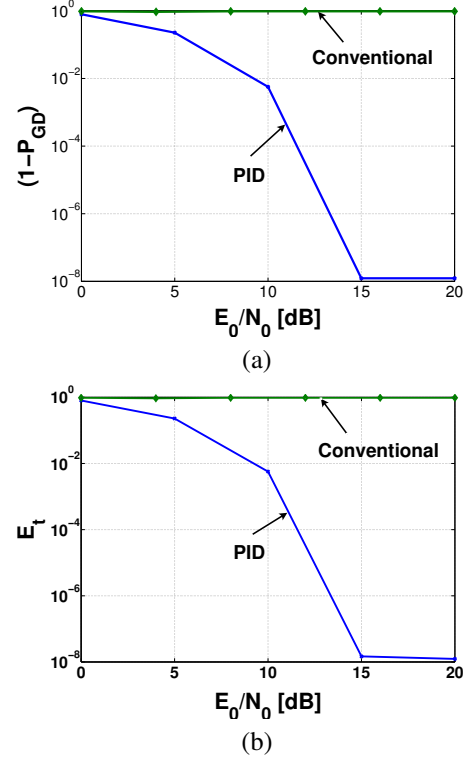

(a)

(b)

Figure 4: A comparison between the PID and the conventional synchronization methods. Exact value for the PID method at the optimal working points, lower bound for the conventional method. (a) $\overline{P_{GD}}$ (the complement of the probability of Good Detection) and (b) $E_t = \overline{P_{GD}} + P_{FA0}$ (the total error). $L_c = 20$, 10 users, A = 10 and B = 7.

functions of E_0/N_0 in dB. The first curve (according to the order in the legend) corresponds to the PID synchronization method. It represents $\overline{P_{GD}}$ values at the optimal working points and that are obtained in the same way as in the section above. Corresponding values of E_t are shown in Fig. 4 (b). The second curve gives the lower bound of $\overline{P_{GD}}$ values for the conventional complete method. The simulated scenario corresponds to 10 users, $L_c = 20$, $A = 10$ and $B = 7$ (A and B do not concern the second curve in Fig. 4 (a)). As we can notice, The PID synchronization method $\overline{P_{GD}}$ is decreasing with E_0/N_0 and it is very small when E_0/N_0 becomes larger than 10 dB. In contrast, with the conventional complete method, $\overline{P_{GD}}$ is very high and it is of 0.97 approximately even when $E_0/N_0 = 20\,dB$. E_t in Fig. 4 (b) is a decreasing function of E_0/N_0, it reaches 10^{-8}

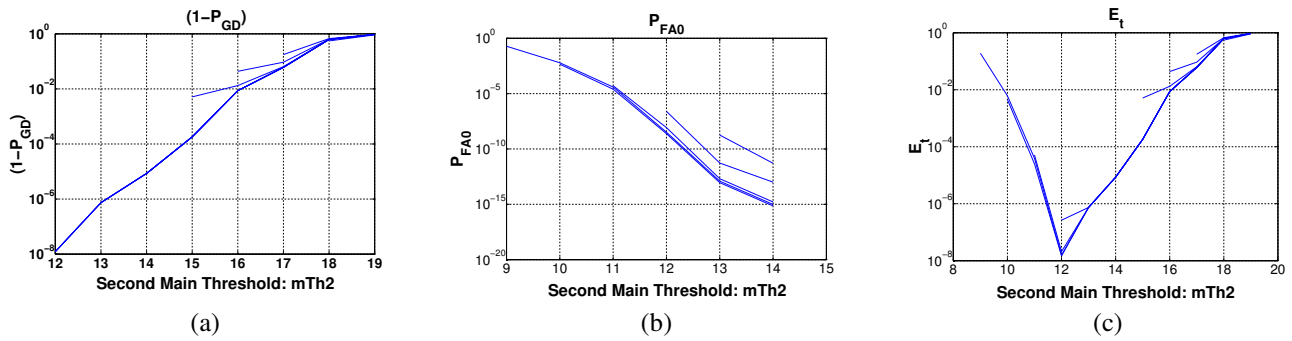**Figure 3:** Performance of PID for various values of the two thresholds mTh1 and mTh2 defined in Section 5.1; mth2 is on the x-axis, mTh1 is the x-value of the leftmost point on each curve. The y-axis shows: (a) $\overline{P_{GD}}$ (the complement of the probability of Good Detection), (b) P_{FA0} (the probability of False Alarm) and (c) $E_t = \overline{P_{GD}} + P_{FA0}$ (the total error). $E_0/N_0 = 15$ dB, $L_c = 20$, 10 users, A = 10 and B = 7.

for $E_0/N_0 = 15\,dB$, whereas it is lower bounded by the lower bound of $\overline{P_{GD}}$, that is 0.97, with the conventional method.

To summarize this section, we have shown that, with the PID synchronization method, the synchronization is achieved with a total error that reaches 10^{-8} in the shown scenarios. In contrast, with the conventional complete method, the total error is very close to 1, which means a certain failure. The PID synchronization method detects only one of the multipath components. Detecting other multipath using PID method is left for future work.

References

[1] U.S. patent application Ser. No. 6,556,621 B1. Richards et al.. Time Doamain Corporation, Huntsville, AL (US). Filed Apr. 29, 2003.

[2] "802.15.4a Channel Model Subgroup Final Report". IEEE P802.15-04-0535-00-004a, September 2004.

[3] "Channel Modeling Sub-Committee Report Final". IEEE P802.15-02/490r1-SG3a, February 2003.

[4] M.-G. Di Benedetto, L. De Nardis, M. Junk, G. Giancola. "(UWB)$\hat{2}$: Uncoordinated, Wireless, Baseborn, medium access control for UWB communication networks". Mobile Networks and Applications special issue on WLAN Optimization at the MAC and Network Levels (2005).

[5] A. El Fawal, J. Y. Le Boudec. "Fast Synchronization in UWB Self-Organized Networks and in the Absence of Power Control". Doctoral School Project, EPFL, July 2004.

[6] J. Foerster and Q. Li. "UWB Channel Modeling Contribultion from Intel". Call for Contributions on Ultra-wideband Channel Models (IEEE P802/208r1-SG3a). Submitted: 24 June, 2002.

[7] Sinan Gezici, Eran Fishler, Hisashi Kobayashi, H. Vincent Poor, and Andreas F. Molisch. "A Rapid Acquisition Technique for Impulse Radio". A MITSUBISHI ELECTRIC RESEARCH LABORATORY, TR-2003-46 August 2003.

[8] S. S. Ghassemzadeh, R. Jana, C. Rice, W. Turin and V. Tarokh. "Measurement and modeling of an ultra-wide bandwidth indoor channel". IEEE TRANSACTIONS ON COMMUNICATIONS, VOL. 52, NO. 10, OCTOBER 2004.

[9] N. He, C. Tepedelenlioglu. "Adaptive Synchronization for Non-Coherent UWB Receivers". IEEE International Conference on Acoustics, Speech and Signal Processing, vol. 4, Pages:iv-517 - iv-520, Montreal, Quebec, Canada, May 17-21, 2004.

[10] E. A. Homier and R. A. Scholtz. "Hybrid Fixed-Dwell-Time Search Techniques for Rapid Acquisition of Ultra-Wideband Signals". International Workshop on Ultra-Wideband Systems, Oulu, Finland June 2-5, 2003.

[11] E. A. Homier and R. A. Scholtz. "Rapid Acquisition of Ultra-wideband Signals in the Dense Multipath Channel". IEEE Conference on Ultra Wideband Systems and Technologies, 2002.

[12] B. Kannan et al.."UWB Channel Caracterization in Indoor Office Environments". IEEE P802.15-15-04-0439-00-004a, August 2004.

[13] R. Merz, J. Widmer, J. Y. Le Boudec, B. Radunovic. "A Joint PHY/MAC Architecture for Low-Radiated Power TH-UWB Wireless Ad-Hoc Networks". To appear in Wireless Communications and Mobile Computing Journal, Special Issue on Ultrawideband (UWB) Communications, 2005.

[14] A. Muqattash and K. Marwan. "CDMA-based MAC protocol for Wireless ad hoc networks". In Proceeding of MOBIHOC'03, pages 153-164, June 2003.

[15] M. Pausini, G.J.M. Janssen. "Analysis and Comparison of Autocorrelation Receivers for IR-UWB Signals Based on Differential Detection". Proc. IEEE Int. Conf. on Acoustics, Speech and Signal Processing, ICASSP 2004, pp. IV513 - IV516, Montreal, Canada, May 2004.

[16] A. Polydoros, C. Weber. "A Unified Approach to Serial Search Spread-Spectrum Code Acquisition–Part I: General Theory". IEEE TRANSACTIONS ON COMMUNICATIONS, VOL. COM-32, NO. 5, MAY 1984.

[17] L. Reggiani and G. M. Maggio. "A Reduced-Complexity Acquisition Algorithm for UWB Impulse Radio". In Proceedings of UWBST 2003, Reston, VA, Nov. 2003.

[18] Z. Tian, L. Yang, and G. B. Giannakis. "Symbol Timing Estimation in Ultra-Wideband Communications". In Proc. of 36th Asilomar Conf. on Signals, Systems, and Computers, pp. 1924-1928, Pacific Grove, CA, November 3-6, 2002.

[19] M. Villanti, M Sabattini, G. M. Maggio, L. B. Milstein. " Non-Coherent Code Acquisition for UWB-IR Systems in Dense Multipath Fading Channels". J-SAC 2004.

[20] L. Yang, G. B. Giannakis. "Blind UWB Timing with a Dirty Template". IEEE International Conference on Acoustics, Speech and Signal Processing, vol. 4, pp. 509-512, Montreal, Quebec, Canada, May 17-21, 2004.

[21] Moe Z. Win, Robert A. Scholtz. "Ultra-Wide Bandwidth Time-Hopping Spread-Spectrum Impulse Radio for Wireless Multiple-Access Communications". IEEE TRANSACTIONS ON COMMUNICATIONS, VOL. 48, NO. 4, APRIL 2000.

[22] M. Z. Win, R. A. Scholtz, and M. A. Barnes. "Ultra-wide bandwidth signal propagation for indoor wireless communications". In Proc. IEEE Int. Conf. Communications, vol. 1, Montral, Canada, June 1997, pp. 56 60.

Appendix

A   Pulse

The second derivative Gaussian pulse is presented in Fig. 5 and it is given by:

$$p(t) = rect_{T_p}(t) \times \left(1 - 4\pi \frac{t^2}{\tau^2} \right) e^{-\frac{2\pi t^2}{\tau^2}} \tag{12}$$

where T_p is the pulse width, τ is the shape factor and the function $rect_{T_p}(t)$ is defined by:

$$rect_{T_p}(t) = \begin{cases} 1 & -\frac{T_p}{2} \leq t \leq \frac{T_p}{2} \\ 0 & Else \end{cases} \tag{13}$$
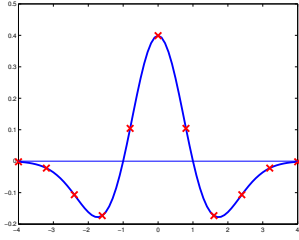

Figure 5: Second derivative Gaussian pulse.

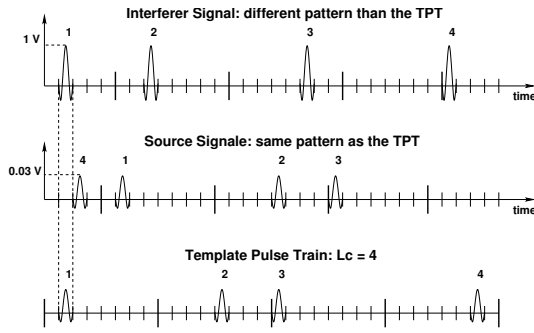# B The Problem with the Conventional Synchronization Method

Figure 6: A scenario showing the problem with the conventional synchronization method. The Source signal has the same pattern as the TPT but shifted in time. The interferer signal, which is 33 times stronger than the source signal, has one pulse aligned with one pulse of the TPT.

Fig. 6 illustrates the scenario of section 3.2 with $L_c = 4$. The source signal has the same pattern as the TPT but it is shifted in time. Corresponding pulses in the TPT and the source signal carry the same number. As we notice there is one interferer pulse (pulse number 1 of the interferer signal) that is aligned with pulse number 1 of the TPT. In this case, a FA will occur since the code length L_c is very small compared to the ratio between the source and the interferer signals.

C Adopted Synchronization Method

In this appendix we show the flowchart for the PID synchronization method. Figs. 7 and 8 illustrate the first and the second phases respectively. The flowchart of the conventional synchronization method can be deduced from Figs. 7 and 8 by simply relaxing the threshold check on the elementary correlation outputs.
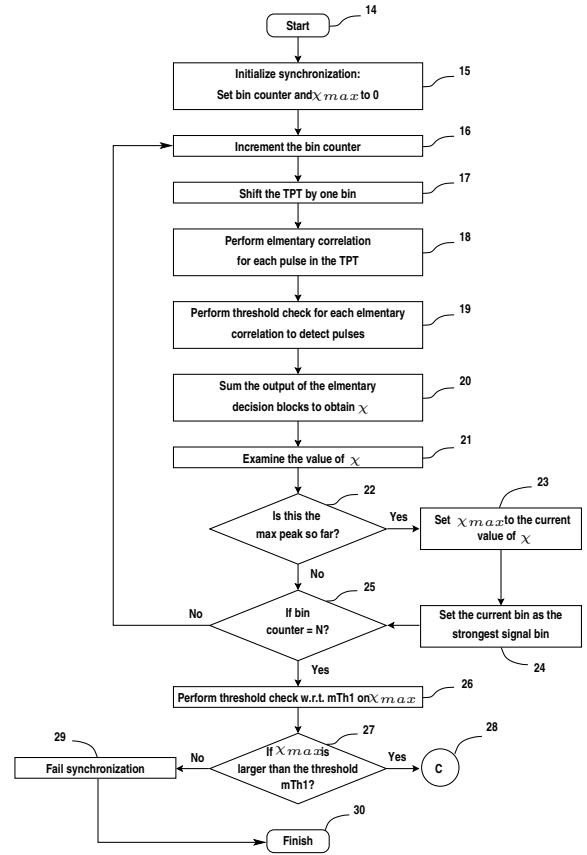

Figure 7: The first phase of the PID synchronization method that finds the signal bin, SB, that corresponds to the highest value of χ above the first main threshold mTh1.

D Analysis

Our analysis treats 3 random variables, X, Y and Z, as it is dictated in Fig. 9. Block 1 represents the first phase in our synchronization method and block 2 illustrates the second phase. X is the input of block 1. Y forms the output of block 1 and the input of block 2. Z is the output of block 2. The values that X, Y and Z can take are as follows:

$$X = \begin{cases} 1 & \text{The IR signal contains the true sequence} \\ 0 & \text{Else} \end{cases}$$

$$Y = \begin{cases} 1 & \text{Good detection and X = 1} \\ 2 & \text{Bad detection either X = 0 or X = 1} \\ 3 & \text{No detection and X = 0} \\ 4 & \text{No detection and X = 1} \end{cases}$$
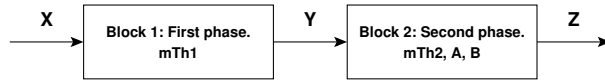
7

Figure 9: The synchronization method is modeled as 2 blocks with 3 random variables. Blocks 1 and 2 represents the first and the second phases respectively. X (input of block 1) indicates the presence of the true sequensce in the received IR signal. Y (output of block 1 and input of block 2)indicates whether a detection is declared or not and, if a detection is declared, whether it is a good detection or a FA. Z (output of block 2) gives the result of the verification of the second phase.

$$Z = \begin{cases} 1 & \text{Good detection: } Y = 1 \text{ and the detection} \\ & \text{is confirmed by the second phase.} \\[1em] 2 & \text{False Alarm: } Y = 2 \text{ and the detection is} \\ & \text{confirmed by the second phase.} \\[1em] 3 & Y = 1 \text{ but the detection is canceled by} \\ & \text{the second phase.} \\[1em] 4 & Y = 2 \text{ but the detection is canceled by} \\ & \text{the second phase.} \end{cases}$$

We have by definition:

$$P_{GD} = P(Z = 1|X = 1) \tag{14}$$
$$P_{FA0} = P(Z = 2|X = 0) \tag{15}$$

Introducing the variable Y in Eq. 14 we can write:

$$P(Z = 1|X = 1) =$$
$$P(Z = 1|Y = 1, X = 1)P(Y = 1|X = 1) +$$
$$P(Z = 1|Y \neq 1, X = 1)P(Y \neq 1|X = 1)$$
$$= P(Z = 1|Y = 1, X = 1)P(Y = 1|X = 1) \tag{16}$$

Similarly we have for Eq. 15:

$$P(Z = 2|X = 0) =$$
$$P(Z = 2|Y = 2, X = 0)P(Y = 2|X = 0) \tag{17}$$

Let us express the terms on the right hand in Eq. 16 and Eq. 17 in term of P_i, $i = 1, \ldots, 4$; By definition we have:

$$P(Y = 1|X = 1) = P_1 \tag{18}$$

$$P(Y = 2|X = 0) = P_2 \tag{19}$$

$$P(Z = 1|Y = 1, X = 1) =$$
$$\sum_{i=B}^{A} \binom{A}{i} P_3^i (1 - P_3)^{(A-i)} \tag{20}$$

$$P(Z = 2|Y = 2, X = 0) =$$
$$\sum_{i=B}^{A} \binom{A}{i} P_4^i (1 - P_4)^{(A-i)} \tag{21}$$

Plugging Eqs. 18 - 21 in Eqs. 16 and 17 we obtain Eqs. 10 and 11.

E Communication Range

The mean channel pathloss excluding antenna effects is defined as [2, 8]

$$PL(d) = \frac{P_{TX}}{E\{P_{RX}(d)\}} \tag{22}$$

where P_{TX} and P_{RX} are transmit and receive power, respectively, d is the distance between the transmitter and the receiver, and the expectation is taken over an area that is large enough to allow averaging out of the shadowing as well as the small-scale fading. Due to the frequency dependence of propagation effects in a UWB channel, the wideband pathloss is a function of frequency as well as distance. The patloss as a function of distance and frequency can be written as a product of the terms

$$PL(f, d) = PL(f)PL(d). \tag{23}$$

The distance dependence of the pathloss in dB is described by

$$PL(d) = PL_0 + 10nlog_{10}\left(\frac{d}{d_0}\right) \tag{24}$$

where the reference distance d_0 is set to 1 m, and PL_0 is the pathloss at the reference distance. n is the pathloss exponent that is equal to 1.63 in the LOS indoor office environment. Then a difference of 20 dB in the pathloss between the source and an interferer that is one meter far from the receiver can be written as:

$$20 = \left(PL_0 + 10nlog_{10}\left(\frac{d_s}{d_0}\right)\right)_s - \left(PL_0 + 10nlog_{10}\left(\frac{d_i}{d_0}\right)\right)_i \tag{25}$$

the indexes s and i are to indicate the source and the interferer respectively. Resolving Eq. 25 we get:

$$d_s = 16.86 \, m \tag{26}$$

F Some Definitions

Search bin: In all cross-correlation based synchronization methods, the synchronization sequence is divided into N search bins. The bin width is equal to a small fraction of the pulse wavelength. If σ is the bin width, we have $N = L_c \times PRP \times T_c/\sigma \, bins$. The TPT shift offset is multiple of the bin width and it determines which bin to be searched, i.e to which bin the TPT

```
            ( C )
              |
  ┌─────────────────────────────────┐
  │ Set successful iteration counter = 0 │
  │   Initialize verification phase,     │
  │     Set iteration counter = 0        │
  └─────────────────────────────────┘
              |
  ┌─────────────────────────────────┐
  │         Set χmax = 0              │
  └─────────────────────────────────┘
              |
  ┌─────────────────────────────────┐
  │   Repeat Blocks from 16 to 25 on   │
  │ a neighborhood V of the detected bin │
  └─────────────────────────────────┘
              |
  ┌─────────────────────────────────┐
  │ Perform threshold check on w.r.t mTh2 │
  └─────────────────────────────────┘
```
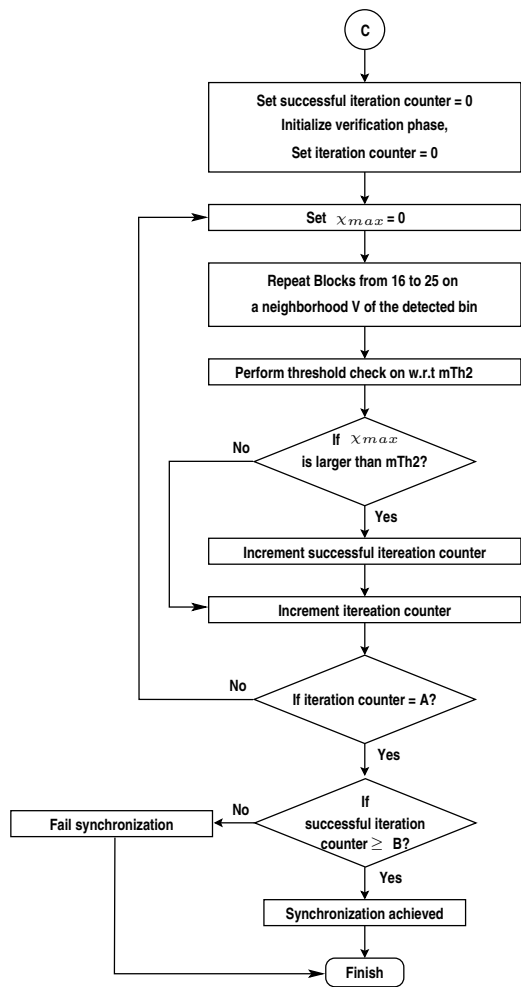
Figure 8: The second phase of the PID synchronization method that verifies the detection declared in the first phase. It consists of A iterartions similar to the first phase but applied on a predefined neighborhood of SB and with a higher second main threshold mTh2..

is shifted. We refer by phase to the bin being searched and by signal bin to the bin that corresponds to a match between the TPT and the received IR signal.

9